Two-fluid magnetic island dynamics in slab geometry: Determination of the island phase velocity

R. Fitzpatrick, P. G. Watson, and F. L. Waelbroeck
Institute for Fusion Studies, Department of Physics, University of Texas at Austin, Austin, Texas 78712

(Received 25 March 2005; accepted 15 June 2005; published online 12 August 2005)

The physics which determines the phase-velocity of a comparatively wide, isolated, magnetic island, formed as a result of a nonlinear tearing instability in a magnetic confinement device relying on the existence of nested magnetic flux surfaces, is investigated using a two-fluid model in slab geometry. It is found that the phase velocity is fixed by *momentum transport* across the magnetic flux surfaces in the region immediately surrounding the magnetic separatrix. Analytic predictions for the phase velocity are obtained, and are successfully benchmarked against the results of two-dimensional, drift-magnetohydrodynamical simulations. © *2005 American Institute of Physics*.
[DOI: 10.1063/1.2001644]

I. INTRODUCTION

Tearing modes are magnetohydrodynamical (MHD) instabilities which often limit fusion plasma performance in magnetic confinement devices, such as tokamaks, which rely on the existence of nested toroidal magnetic flux surfaces.[1] As the name suggests, "tearing" modes tear and reconnect magnetic field lines, in the process converting nested toroidal flux surfaces into helical magnetic islands. Such islands degrade plasma confinement because heat and particles are able to travel radially from one side of an island to another by flowing along magnetic field lines, which is a relatively fast process, instead of having to diffuse across magnetic flux surfaces, which is a relatively slow process.[2]

In two-fluid MHD theory, which is far more relevant to present-day magnetic confinement devices than single-fluid MHD theory, a magnetic island is embedded within ion and electron fluids which generally flow at *different* velocities. The island itself usually propagates at some intermediate velocity. For a sufficiently wide island (i.e., much wider than the collisionless ion skin depth), both fluids are required to flow at the island propagation velocity in the region lying within the magnetic separatrix (since neither fluid can easily cross the separatrix, or any other magnetic flux surface). However, the region immediately outside the separatrix is characterized by strongly sheared ion and electron fluid flow profiles, as the velocities of both fluids adjust to their unperturbed values far away from the island. The polarization current generated by the strongly sheared ion flow around the island separatrix gives rise to an additional term[3] in the well-known Rutherford island width evolution equation,[4] which takes the normalized (see Sec. II A) form

$$\frac{0.823}{\eta}\frac{dW}{dt} = \Delta' + \Delta_{polz} \tag{1}$$

in *slab* geometry. Here, W is the full island width, η the local plasma resistivity, Δ' the conventional tearing stability index,[5] and

$$\Delta_{polz} = 1.38\frac{(V - V_{EB})(V - V_i)}{(W/4)^3} \tag{2}$$

the ion polarization term.[6] In the above, V is the island phase velocity, V_{EB} the unperturbed (i.e., in the absence of an island) local $\mathbf{E}\times\mathbf{B}$ velocity, and V_i the unperturbed local ion fluid velocity. The polarization term can be significant in present-day magnetic confinement devices, and is stabilizing when the island phase velocity lies between the unperturbed local ion fluid and $\mathbf{E}\times\mathbf{B}$ velocities,[7] and destabilizing otherwise.

It follows, from the above discussion, that the determination of the phase velocity is a vital element in two-fluid magnetic island theory, since without this knowledge it is impossible to say whether the ion polarization term in the Rutherford equation is stabilizing or destabilizing.

In Ref. 6, a set of reduced, two-dimensional (2D), drift-MHD equations was developed, and this set of equations then used to investigate magnetic island dynamics in slab geometry. For comparatively wide, *isolated* islands, a very simple result was obtained for the island phase velocity—the phase velocity is the (perpendicular) *viscosity weighted mean* of the unperturbed local ion and electron fluid velocities, i.e.,

$$V = \frac{\mu_i V_i + \mu_e V_e}{\mu_i + \mu_e}. \tag{3}$$

Here, V_e is the unperturbed local electron fluid velocity, and $\mu_{i,e}$ are the local (perpendicular) ion and electron fluid viscosities. However, the derivation of the above result is only valid in the "subsonic" limit,

$$kV_* \ll k_\parallel c_s, \tag{4}$$

where V_* is the unperturbed local diamagnetic velocity, k the island wave number, $k_\parallel$ the parallel (to the magnetic field) wave number calculated at the edge of the island, and c_s the local sound speed.

The aim of this paper is to extend the analysis of Ref. 6, so as to determine the phase velocity of isolated magnetic islands in situations where the inequality (4) is no longer satisfied. For the sake of simplicity, all of our analysis is

performed in slab geometry. We shall also compare our analytical predictions with the results of nonlinear, 2D, drift-MHD simulations.

This paper is organized as follows. All of our analysis is in Sec. II. Section III contains a review of previously published work on the phase velocity of comparatively wide, isolated, drift-MHD magnetic islands in slab geometry. Next, in Sec. IV, we compare our analytical results with the results of nonlinear, 2D, drift-MHD simulations. Finally, we summarize and draw conclusions in Sec. V.

II. ANALYSIS

A. Reduced equations

Standard right-handed Cartesian coordinates (x,y,z) are adopted. Consider a quasi-neutral plasma with singly charged ions of mass m_i. The ion/electron number density n_0 is assumed to be *uniform* and *constant*. Suppose that $T_i = \tau T_e$, where $T_{i,e}$ is the ion/electron temperature, and τ is uniform and constant. Let there be no variation of quantities in the z direction, i.e., $\partial/\partial z \equiv 0$. Finally, let all lengths be normalized to a, which is the typical variation length scale of B_y; let all magnetic field strengths be normalized to B_a, which is the typical strength of B_y away from the resonant surface; and let all times be normalized to a/V_a, where $V_a = B_a/\sqrt{\mu_0 n_0 m_i}$.

We can write $\mathbf{B} = \nabla\psi\times\hat{\mathbf{z}} + (B_0 + b_z)\hat{\mathbf{z}}$, and $P = P_0 - B_0 b_z + O(1)$, where $\mathbf{B}$ is the magnetic field, and P the total plasma pressure. Here, we are assuming that P_0 and B_0 are uniform, and $P_0 \gg B_0 \gg 1$, with ψ and b_z both $O(1)$.[6] When expressed in unnormalized quantities, our fundamental ordering takes the form

$$\frac{\mu_0 P_0}{B_a^2} \gg \frac{B_0}{B_a} \gg 1. \tag{5}$$

Let $\beta = \Gamma P_0/B_0^2$ be (Γ times) the plasma beta calculated with the "guide field," B_0, where $\Gamma = 5/3$ is the plasma ratio of specific heats. Note that the above ordering scheme (which is effectively a high poloidal beta scheme, i.e., $\mu_0 P_0/B_a^2 \gg 1$, in unnormalized units) does not constrain β (which is effectively the toroidal beta) to be either much less than or much greater than unity.

We adopt the reduced, 2D, drift-MHD equations derived in Ref. 6:

$$\frac{\partial\psi}{\partial t} = [\phi - Z, \psi] + \eta J - \mu_e(1+\tau)\nabla^2[V_z + (d_\beta/c_\beta)^2 J], \tag{6}$$

$$\frac{\partial Z}{\partial t} = [\phi, Z] + c_\beta^2[V_z, \psi] + d_\beta^2[J, \psi] + D\nabla^2 Z + \mu_e d_\beta^2 \nabla^4(\phi - Z), \tag{7}$$

$$\frac{\partial\nabla^2\phi}{\partial t} = [\phi, \nabla^2\phi] - \frac{\tau}{2}(\nabla^2[\phi, Z] + [\nabla^2\phi, Z] + [\nabla^2 Z, \phi]) + [J, \psi] + \mu_i\nabla^4(\phi + \tau Z) + \mu_e\nabla^4(\phi - Z), \tag{8}$$

$$\frac{\partial V_z}{\partial t} = [\phi, V_z] + [Z, \psi] + \mu_i\nabla^2 V_z + \mu_e\nabla^2[V_z + (d_\beta/c_\beta)^2 J], \tag{9}$$

where $J = 1 + \nabla^2\psi$, and $D = c_\beta^2\eta + (1 - c_\beta^2)\kappa$. Here, $c_\beta = \sqrt{\beta/(1+\beta)}$, $d_\beta = c_\beta d_i/\sqrt{1+\tau}$, $Z = d_i b_z/(1+\tau)$, $d_i = (m_i/n_0 e^2\mu_0)^{1/2}/a$, and $[A, B] = \nabla A \times \nabla B \cdot \hat{\mathbf{z}}$. Of course, d_i is the (normalized) collisionless ion skin depth. Note that the (normalized) length d_β reduces to the (normalized) *collisionless ion skin depth*, d_i, in the limit $\beta \gg 1$, and to the (normalized) *sonic ion gyroradius*, $\rho_s = \sqrt{\beta} d_i$, in the limit $\beta \ll 1$. The guiding-center velocity is written as $\mathbf{V} = \nabla\phi\times\hat{\mathbf{z}} + d_i(c_\beta/d_\beta)^2 V_z\hat{\mathbf{z}}$. The ion fluid velocity is written as $\mathbf{V}_i = \nabla(\phi + \tau Z)\times\hat{\mathbf{z}} + d_i(c_\beta/d_\beta)^2 V_z\hat{\mathbf{z}}$. Finally, the electron fluid velocity is written as $\mathbf{V}_e = \nabla(\phi - Z)\times\hat{\mathbf{z}} + d_i(c_\beta/d_\beta)^2[V_z + (d_\beta/c_\beta)^2 J]\hat{\mathbf{z}}$. Furthermore, η is the (uniform) plasma resistivity, $\mu_{i,e}$ the (uniform) ion/electron viscosity, and κ the (uniform) plasma thermal conductivity. The above equations contain both electron and ion diamagnetic effects, including the contribution of the anisotropic ion gyroviscous tensor, but neglect electron inertia. Our equations are "reduced" in the sense that they do not contain the compressible Alfvén wave. However, they do contain the shear-Alfvén wave, the magnetoacoustic wave, the whistler wave, and the kinetic-Alfvén wave. Note that the transport coefficients, μ_i, μ_e, and κ, appearing in the above equations, are *phenomenological* in nature, and are supposed to represent the anomalous *diffusive* transport of momentum and energy across magnetic flux surfaces due to small-scale plasma turbulence.

B. Island geometry

Consider a *slab* plasma which is periodic in the y direction with periodicity length l. Let the system be *symmetric* about $x=0$, i.e., $\psi(-x,y,t) = \psi(x,y,t)$, $Z(-x,y,t) = -Z(x,y,t)$, $\phi(-x,y,t) = -\phi(x,y,t)$, and $V_z(-x,y,t) = V_z(x,y,t)$. Consider a saturated, constant-ψ magnetic island, centered on $x=0$. It is convenient to transform to the *island rest-frame*, in which $\partial/\partial t \equiv 0$. Suppose that the island is embedded in a plasma with *uniform* (but different) y-directed ion and electron fluid velocities. We are searching for an island solution in which the ion/electron fluid velocities asymptote to these uniform velocities far from the magnetic separatrix.

In the immediate vicinity of the island, we can write

$$\psi(x,\theta) = -\frac{x^2}{2} + \Psi\cos\theta, \tag{10}$$

where $\theta = ky$, $k = 2\pi/l$, and $\Psi > 0$ is the reconnected magnetic flux. As is well known, the above expression for ψ describes a "cat's eye" magnetic island of full-width (in the x direction) $W = 4w$, where $w = \sqrt{\Psi}$. The region inside the magnetic separatrix corresponds to $\Psi \geq \psi > -\Psi$, whereas the region outside the separatrix corresponds to $\psi < -\Psi$.

It is helpful to define a flux-surface average operator:

$$\langle f(s,\psi,\theta)\rangle = \oint \frac{f(s,\psi,\theta)}{|x|}\frac{d\theta}{2\pi} \tag{11}$$

for $\psi < -\Psi$, and

$$\langle f(s,\psi,\theta)\rangle = \int_{-\theta_0}^{\theta_0} \frac{f(s,\psi,\theta)+f(-s,\psi,\theta)}{2|x|}\frac{d\theta}{2\pi} \tag{12}$$

for $\Psi \geqslant \psi > -\Psi$. Here, $s=\mathrm{sgn}(x)$, and $x(s,\psi,\theta_0)=0$ (with $\pi > \theta_0 > 0$). The most important property of this operator is that $\langle [A,\psi]\rangle \equiv 0$ for any field $A(s,\psi,\theta)$.

C. Ordering scheme

Let $\eta=\epsilon\hat{\eta}$, $D=\epsilon\hat{D}$, and $\mu_{ie}=\epsilon\hat{\mu}_{i,e}$, where

$$\epsilon \ll d_\beta^2 \ll 1. \tag{13}$$

The above ordering scheme assumes that the (unnormalized) length d_β is much smaller than the typical variation length scale of the equilibrium, and that transport terms are extremely small compared to the other terms in our equations. These assumptions are appropriate to high-temperature fusion plasmas.

In the island rest frame, Eqs. (6)–(9) yield

$$0=[\phi-Z,\psi]+\epsilon\hat{\eta}J-\epsilon\hat{\mu}_e(1+\tau)\nabla^2[V_z+(d_\beta/c_\beta)^2J], \tag{14}$$

$$0=[\phi,Z]+c_\beta^2[V_z,\psi]+d_\beta^2[J,\psi]+\epsilon\hat{D}\nabla^2Z + \epsilon\hat{\mu}_e d_\beta^2\nabla^4(\phi-Z), \tag{15}$$

$$0=[\phi,\nabla^2\phi]-\frac{\tau}{2}(\nabla^2[\phi,Z]+[\nabla^2\phi,Z]+[\nabla^2Z,\phi])+[J,\psi] + \epsilon\hat{\mu}_i\nabla^4(\phi+\tau Z)+\epsilon\hat{\mu}_e\nabla^4(\phi-Z), \tag{16}$$

$$0=[\phi,V_z]+[Z,\psi]+\epsilon\hat{\mu}_i\nabla^2V_z+\epsilon\hat{\mu}_e\nabla^2[V_z+(d_\beta/c_\beta)^2J]. \tag{17}$$

All quantities in the above equations are assumed to be $O(1)$, except for the small parameters d_β^2 and ϵ. Let

$$\phi(x,\theta)=s[\phi_0(\psi)+d_\beta^2\phi_c(\psi,\theta)+\epsilon\phi_s(\psi,\theta)], \tag{18}$$

$$Z(x,\theta)=s[Z_0(\psi)+d_\beta^2Z_c(\psi,\theta)+\epsilon Z_s(\psi,\theta)], \tag{19}$$

$$V_z(x,\theta)=d_\beta^2V_c(\psi,\theta)+\epsilon V_s(\psi,\theta), \tag{20}$$

$$J(x,\theta)=J_0(\psi,\theta)+d_\beta^2J_c(\psi,\theta)+\epsilon J_s(\psi,\theta). \tag{21}$$

Here, the subscript c indicates that the associated quantity has the symmetry of $\cos\theta$, whereas the subscript s indicates that the associated quantity has the symmetry of $\sin\theta$. Note that ϕ_0 and Z_0 must both be zero inside the island separatrix, since it is impossible to have a nonzero odd (in x) flux-surface function in this region.

D. Analysis

The lowest-order component of Eq. (16) with the symmetry of $\sin\theta$ yields

$$0=[\phi_0,\nabla^2\phi_0]-\frac{\tau}{2}([\nabla^2\phi_0,Z_0]+[\nabla^2Z_0,\phi_0])+[J_0,\psi] + O(d_\beta^2). \tag{22}$$

Writing $M(\psi)=d\phi_0/d\psi$ and $L(\psi)=dZ_0/d\psi$, the above expression reduces to

$$\tilde{J}_0=\frac{1}{2}\frac{d[M(M+\tau L)]}{d\psi}\widetilde{x^2}, \tag{23}$$

where $\tilde{A}\equiv A-\langle A\rangle/\langle 1\rangle$. Note that the (normalized) electron fluid, $\mathbf{E}\times\mathbf{B}$, and ion fluid velocities in the y direction are given by $V_e=|x|(M-L)$, $V_{EB}=|x|M$, and $V_i=|x|(M+\tau L)$, respectively.

The lowest order components of Eqs. (14), (15), and (17) with the symmetry of $\sin\theta$ are

$$0=[\phi_c-Z_c,\psi]+O(d_\beta^2), \tag{24}$$

$$0=[\phi_c,Z_0]+[\phi_0,Z_c]+c_\beta^2[V_c,\psi]+[J_0,\psi]+O(d_\beta^2), \tag{25}$$

$$0=[\phi_0,V_c]+[Z_c,\psi]+O(d_\beta^2). \tag{26}$$

These equations can be solved to give

$$\tilde{\phi}_c=\tilde{Z}_c=M\tilde{V}_c=-\frac{[M(M+\tau L)]'/2}{L-M+c_\beta^2/M}\widetilde{x^2}, \tag{27}$$

where $'$ denotes $d/d\psi$.

The lowest-order components of Eqs. (14), (15), and (17) with the symmetry of $\cos\theta$ are

$$0=[\phi_s-Z_s,\psi]+\hat{\eta}J_0+O(d_\beta^2), \tag{28}$$

$$0=[\phi_s,Z_0]+[\phi_0,Z_s]+c_\beta^2[V_s,\psi]+D\nabla^2Z_0+O(d_\beta^2), \tag{29}$$

$$0=[\phi_0,V_s]+[Z_s,\psi]+O(d_\beta^2). \tag{30}$$

The flux-surface averages of Eqs. (28) and (29) yield

$$\langle J_0\rangle=0 \tag{31}$$

and

$$\langle\nabla^2Z_0\rangle=\langle x^2\rangle\frac{dL}{d\psi}-\langle 1\rangle L=0, \tag{32}$$

respectively. The solution to the above equation, subject to the boundary condition $|x|L\to V_*/(1+\tau)$ as $|x|/w\to\infty$, where V_* is the unperturbed (normalized) total diamagnetic velocity in the y direction, is

$$L(\psi)=\frac{V_*}{(1+\tau)}\frac{1}{\langle x^2\rangle} \tag{33}$$

outside the separatrix. Of course, $L(\psi)=0$ inside the separatrix. The apparent discontinuity in $L(\psi)$ is mediated by a thin boundary layer on the separatrix, which can be resolved by including higher-order terms in Eqs. (28)–(30).[6]

Equations (28)–(30) can be solved to give

$$[\phi_s,\psi]=-\left(\frac{\hat{\eta}[c_\beta^2/M-M][M(M+\tau L)]'/2+\hat{D}L'}{L-M+c_\beta^2/M}\right)\widetilde{x^2}, \tag{34}$$

$$[Z_s,\psi]=M[V_s,\psi]=\left(\frac{\hat{\eta}L[M(M+\tau L)]'/2-\hat{D}L'}{L-M+c_\beta^2/M}\right)\widetilde{x^2}. \tag{35}$$

The fact that we have obtained sensible expressions for ϕ_c, Z_c, V_c, ϕ_s, Z_s, and V_s demonstrates the validity of the expansion (18)–(21).

The lowest-order flux-surface average of Eq. (16) yields

$$\begin{aligned}0=&\langle[\phi_s,\nabla^2\phi_0]\rangle-\frac{\tau}{2}\{\langle\nabla^2[\phi_s,Z_0]\rangle+\langle\nabla^2[\phi_0,Z_s]\rangle\\&+\langle[\nabla^2\phi_0,Z_s]\rangle+\langle[\nabla^2Z_0,\phi_s]\rangle\}+\hat{\mu}_i\langle\nabla^4(\phi_0+\tau Z_0)\rangle\\&+\hat{\mu}_e\langle\nabla^4(\phi_0-Z_0)\rangle+O(d_\beta^2),\end{aligned} \tag{36}$$

which reduces to

$$\begin{aligned}0=&\frac{d}{d\psi}\{M'\langle\widetilde{x^2}[\phi_s,\psi]\rangle\}-\frac{\tau}{2}\frac{d^2}{d\psi^2}\{L\langle\widetilde{x^2}[\phi_s,\psi]\rangle\\&-M\langle\widetilde{x^2}[Z_s,\psi]\rangle\}+\frac{\tau}{2}\frac{d}{d\psi}\{M'\langle\widetilde{x^2}[Z_s,\psi]\rangle\\&+L'\langle\widetilde{x^2}[\phi_s,\psi]\rangle\}+\frac{d^2}{d\psi^2}\{\hat{\mu}_i\langle x^4\rangle(M+\tau L)'\\&+\hat{\mu}_e\langle x^4\rangle(M-L)'\}.\end{aligned} \tag{37}$$

Integrating once in ψ, applying the boundary condition $M\to 0$ as $|x|/w\to\infty$, and making use of Eqs. (34) and (35), we obtain

$$\begin{aligned}&\frac{d}{d\psi}\left[\langle x^4\rangle\frac{d}{d\psi}\{(\mu_i+\mu_e)M+(\mu_i\tau-\mu_e)L\}+\frac{\tau}{2}\left\{\frac{\eta c_\beta^2L[M(M+\tau L)]'/2+DM[L-M]L'}{M(L-M)+c_\beta^2}\right\}\langle\widetilde{x^2}\,\widetilde{x^2}\rangle\right]\\&=\left\{\frac{-\eta M([M(M+\tau L)]'/2)^2}{M(L-M)+c_\beta^2}\right\}\langle\widetilde{x^2}\,\widetilde{x^2}\rangle+\left\{\frac{\eta c_\beta^2[M'+\tau L'/2][M(M+\tau L)]'/2+DML'[M'+\tau(L'+M')/2]}{M(L-M)+c_\beta^2}\right\}\langle\widetilde{x^2}\,\widetilde{x^2}\rangle.\end{aligned} \tag{38}$$

The above equation can be solved for $M(\psi)$, subject to the boundary conditions $M=0$ on the separatrix, and $|x|M\to M_0$ as $|x|/w\to\infty$. The constant M_0 determines the island phase velocity, V, relative to the unperturbed $\mathbf{E}\times\mathbf{B}$ velocity in the y direction, V_{EB}, according to the relation

$$V-V_{EB}=-M_0. \tag{39}$$

In the immediate vicinity of the island, it is helpful to perform the following renormalization: $\hat{\psi}=-\psi/\Psi$, $X=x/w$, $\langle\langle\cdots\rangle\rangle=\langle\cdots\rangle w$, $\hat{L}=L/L_0$, and $\hat{M}=M/L_0$, where $L_0=V_*/[w(1+\tau)]$. This renormalization is consistent with our previous ordering scheme provided $\Psi\equiv w^2$, w, and L_0 can all be regarded as $O(1)$ compared to d_β^2. This is easily satisfied, but implies that

$$d_\beta\ll w, \tag{40}$$

i.e., the island width is much greater than d_β. It follows from (33) that

$$\hat{L}(\hat{\psi})=\frac{1}{\langle\langle X^2\rangle\rangle} \tag{41}$$

outside the separatrix (i.e., $\hat{\psi}>1$). Equation (38) becomes

$$\begin{aligned}&\frac{d}{d\hat{\psi}}\left[\langle\langle X^4\rangle\rangle\frac{d}{d\hat{\psi}}\left\{\hat{M}+\left(\frac{\tau-\mu_e/\mu_i}{1+\mu_e/\mu_i}\right)\hat{L}\right\}+\frac{\tau}{2}\left\{\frac{\zeta_1\hat{L}[\hat{M}(\hat{M}+\tau\hat{L})]'/2+\zeta_2\hat{M}[\hat{L}-\hat{M}]\hat{L}'}{\hat{M}(\hat{L}-\hat{M})+\alpha^2}\right\}\langle\langle\widetilde{X^2}\,\widetilde{X^2}\rangle\rangle\right]\\&=\left\{\frac{-\zeta_1\hat{M}([\hat{M}(\hat{M}+\tau\hat{L})]'/2)^2/\alpha^2}{\hat{M}(\hat{L}-\hat{M})+\alpha^2}\right\}\langle\langle\widetilde{X^2}\,\widetilde{X^2}\rangle\rangle+\left\{\frac{\zeta_1[\hat{M}'+\tau\hat{L}'/2][\hat{M}(\hat{M}+\tau\hat{L})]'/2+\zeta_2\hat{M}\hat{L}'[\hat{M}'+\tau(\hat{L}'+\hat{M}')/2]}{\hat{M}(\hat{L}-\hat{M})+\alpha^2}\right\}\\&\quad\times\langle\langle\widetilde{X^2}\,\widetilde{X^2}\rangle\rangle,\end{aligned} \tag{42}$$

where $'$ now denotes $d/d\hat{\psi}$. Here,

$$\alpha=\frac{c_\beta w(1+\tau)}{V_*}, \tag{43}$$

$\zeta_1=\eta c_\beta^2/(\mu_i+\mu_e)$, and $\zeta_2=D/(\mu_i+\mu_e)=\zeta_1+(1-c_\beta^2)\kappa/(\mu_i+\mu_e)$. Note that $\alpha\sim k_\parallel c_s/kV_*$. Equation (42) can be solved for $\hat{M}(\hat{\psi})$, subject to the boundary conditions that $\hat{M}=0$ at $\hat{\psi}=1$, and $|X|\hat{M}\to\hat{M}_0$ as $\hat{\psi}\to\infty$. The constant $\hat{M}_0$ determines the island phase velocity via

$$\frac{V-V_{EB}}{V_*}=-\frac{\hat{M}_0}{1+\tau}. \tag{44}$$

E. The subsonic limit

The limit $\alpha \gg 1$ is examined in detail in Ref. 6. In this limit, $kV_* \ll k_\parallel c_s$, i.e., the propagation rate of sound waves around island flux surfaces is *much greater* than the island frequency (in the local $\mathbf{E}\times\mathbf{B}$ frame). Such an island is termed a "subsonic" island. Let us briefly review the physics of subsonic islands.

In the subsonic limit, $\alpha \gg 1$, Eqs. (41) and (42) reduce to

$$\frac{d}{d\hat{\psi}}\left(\langle\langle X^4\rangle\rangle \frac{d}{d\hat{\psi}}\left[\hat{M} + \frac{(\mu_i\tau - \mu_e)}{(\mu_i + \mu_e)}\frac{1}{\langle\langle X^2\rangle\rangle}\right]\right) \simeq 0, \tag{45}$$

with the boundary conditions $\hat{M}=0$ for $\hat{\psi}<1$, and $|X|\hat{M} \to \hat{M}_0$ as $|X|\to\infty$. The value of $\hat{M}_0$ determines the island phase velocity V via Eq. (44). The appropriate solution to Eq. (45) is $\hat{M}(\hat{\psi})=0$ for $\hat{\psi}<1$, and

$$\hat{M}(\hat{\psi}) \simeq -\frac{(\mu_i\tau - \mu_e)}{(\mu_i + \mu_e)}\frac{1}{\langle\langle X^2\rangle\rangle} \tag{46}$$

for $\hat{\psi}>1$, which implies that

$$V = V_{EB} + \frac{(\mu_i\tau - \mu_e)V_*}{(\mu_i + \mu_e)(1+\tau)} = \frac{\mu_i V_i + \mu_e V_e}{\mu_i + \mu_e}, \tag{47}$$

where $V_i = V_{EB} + [\tau/(1+\tau)]V_*$ is the unperturbed ion fluid velocity in the y direction (i.e., the ion fluid velocity in the absence of an island), and $V_e = V_{EB} - [1/(1+\tau)]V_*$ the unperturbed electron fluid velocity in the y direction (i.e., the electron fluid velocity in the absence of an island). Thus, the island phase velocity is the (perpendicular) *viscosity weighted mean* of the unperturbed local velocities of the ion and electron fluids.[6] As before, the apparent discontinuity in $\hat{M}(\hat{\psi})$ at $\hat{\psi}=1$ is mediated by a thin boundary layer on the separatrix, which can be resolved by including higher-order terms in the analysis in Sec. II D.

Note that (46) is the *only* solution of Eq. (45) which satisfies the large-$|X|$ boundary condition $|X|\hat{M} \to \hat{M}_0$ as $|X| \to \infty$. This boundary condition implies that the island only modifies the ion/electron fluid velocity profiles in the immediate vicinity of the island, i.e., the velocity profiles are *localized*. All other solutions of Eq. (45) satisfy the boundary condition $\hat{M} \to \hat{M}_1$ as $|X|\to\infty$. These solutions have *nonlocalized* velocity profiles, i.e., the island modifies the ion/electron fluid velocity profiles across the *whole* plasma, instead of just in a localized region centered on the island. Naturally, we expect an *isolated* magnetic island to have a *localized* velocity profile. Hence, we conclude that (46) is the *only* allowable solution of Eq. (45) for an isolated island.

Note, also, that our analysis implies that the phase velocity of a drift-MHD magnetic island is determined solely by *momentum transport* across the flux surfaces immediately surrounding the magnetic separatrix. In the subsonic limit, the dominant momentum transport mechanism is (perpendicular) viscosity.

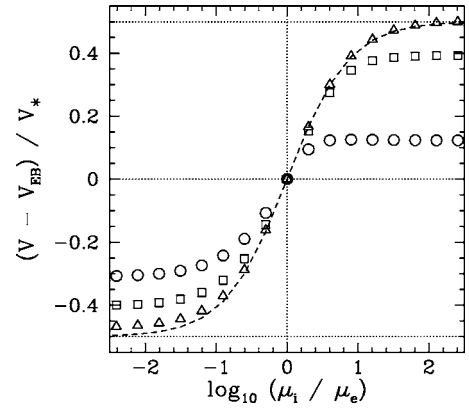

FIG. 1. Steady-state island phase velocity, V, in the local $\mathbf{E}\times\mathbf{B}$ frame, normalized to the total diamagnetic velocity, and evaluated as a function of μ_i/μ_e. The calculations are performed with $D=0.5$ and $\tau=1$. The dashed curve shows the analytic prediction (47) in the subsonic regime, $\alpha \gg 1$. The triangular, square, and circular points show the analytic prediction in the sonic regime, with $\alpha=2$, $\alpha=1$, and $\alpha=0.5$, respectively.

F. The sonic limit

Consider, now, the limit in which $\alpha \sim O(1)$. In this limit, $kV_* \sim k_\parallel c_s$, i.e., the propagation rate of sound waves around island flux surfaces is *similar* to the island frequency (in the local $\mathbf{E}\times\mathbf{B}$ frame). Such an island is termed a "sonic" island.

In the sonic limit, Eq. (42) does not reduce to Eq. (45). Hence, we do not expect the simple analytic result (47) to hold in this case.

We can solve Eq. (42) numerically in a two-stage process. First, we solve in the boundary layer on the separatrix by assuming that $\hat{L}(\hat{\psi})$ takes the form

$$\hat{L}(\hat{\psi}) \simeq \frac{\pi}{4}\left[1 - \exp\left(-\frac{\hat{\psi}-1}{\delta}\right)\right] \tag{48}$$

in the layer, by analogy with the layer solution found in Ref. 6. Here, $\delta \ll 1$. Making use of (48), we can integrate Eq. (42) across the layer, looking for a solution which satisfies $\hat{M}(1)=0$, and $\hat{M}(\hat{\psi}) \to \hat{m}_0$ as $(\hat{\psi}-1)/\delta \to \infty$. Finally, we integrate Eq. (42) outside the layer, with $\hat{L}(\hat{\psi})$ given by (41), subject to the boundary conditions $\hat{M}(1)=\hat{m}_0$, and $|X|\hat{M} \to \hat{M}_0$ as $|X|\to\infty$. This procedure uniquely determines $\hat{M}_0$, and thereby uniquely determines the island phase velocity via Eq. (44). Note that the final answer is independent of the details of the boundary layer, provided $\delta \ll 1$, i.e., provided that the boundary layer is much thinner than the island.

Figure 1 illustrates the results of this method of calculating the island phase velocity in the sonic regime. It can be seen that for $\alpha \gtrsim 2$ the method reproduces the familiar subsonic result (47). However, as α is decreased, and we enter the sonic regime, the island phase velocity shifts toward the local $\mathbf{E}\times\mathbf{B}$ velocity, relative to the subsonic prediction. This velocity shift is somewhat greater for islands propagating in the ion diamagnetic direction (i.e., $V - V_{EB} > 0$), rather than the electron diamagnetic direction.

It is clear, from the analysis in Sec. II D, that the above-mentioned velocity shift is attributable to momentum transport across flux surfaces outside the magnetic separatrix which is associated with *Reynolds stresses*. These stresses develop as a result of small variations of ϕ and Z around flux surfaces which are driven by uneven cross-flux-surface transport. Such variations are smoothed out by sound waves in the subsonic limit.

III. LITERATURE REVIEW

Let us compare our analysis of the island phase-velocity problem with previously published studies. Since we are dealing with a *fluid* treatment of the propagation of comparatively *wide* islands (i.e., $W \gg d_\beta$) in *slab* geometry, we shall restrict the scope of this discussion to those studies of the propagation of wide islands in which toroidal, neoclassical, and kinetic effects do not play a prominent role.

The first paper to seriously address the island phase-velocity problem was Scott *et al.*[8] This paper argues that once the magnetic island width becomes sufficiently large for the island to enter the subsonic regime, sound waves propagating around island flux surfaces flatten the pressure profile inside the separatrix, and that this effectively extinguishes diamagnetic effects. Hence, the prediction of this paper is that magnetic islands in the subsonic regime should propagate at the local $\mathbf{E}\times\mathbf{B}$ velocity. However, this argument needs to be modified in the presence of significant cross-field viscous momentum transport. Although it is true that diamagnetic flow is extinguished *inside* the island separatrix, this is not the case in the region immediately *outside* the separatrix, which is characterized by strongly sheared ion and electron fluid velocity profiles, as the velocities of both fluids adjust to their unperturbed values far away from the island. Momentum transport across flux surfaces outside the separatrix tends to drag the island into the frame of the most viscous fluid, thereby imparting a diamagnetic component to the island velocity. Scott *et al.* present a numerical simulation in justification of their argument. In this simulation, there is no (perpendicular) electron fluid viscosity, but there is a finite (perpendicular) ion viscosity. Furthermore, the ions are cold, so there are no ion diamagnetic effects. In this special case, we predict (along with Scott *et al.*) that the island should propagate at the local $\mathbf{E}\times\mathbf{B}$ velocity, which is exactly what happens in the simulation.

Smolyakov[3] presents a method of calculating the phase velocity of a magnetic island which depends on an energy conservation argument. This method yields results which are quite different to ours. We note, however, that the analysis of Smolyakov completely neglects perpendicular momentum transport, which plays a crucial role in our analysis.

Mikhailovskii *et al.*, have published a long series of papers on magnetic island propagation. The results of these papers are summarized in Mikhailovskii.[9] According to Mikhailovskii and co-workers, a steadily rotating magnetic island is subject to the force-balance constraint:

$$0 = F_{EM} + F_{VS}. \tag{49}$$

Here, F_{EM} is the net electromagnetic force acting on the island, whereas F_{VS} is the net viscous force. However, for an *isolated* island we expect $F_{EM}=0$, since the island cannot exert a net electromagnetic force on itself. Hence, an isolated island satisfies

$$0 = F_{VS}. \tag{50}$$

It follows that the above constraint should be sufficient to determine the phase-velocity of the island. However, we also expect an isolated island to possess a *localized* velocity profile. Furthermore, it is possible to demonstrate that *all* localized velocity profiles satisfy $F_{VS}=0$ *automatically*. Hence, the constraint (50) appears to be incapable of differentiating between different localized velocity profiles, and, hence, of determining the phase velocity of the island. In order to resolve this "paradox," Mikhailovskii and co-workers suggest that time-varying terms should be retained in Eq. (50). This is tantamount to saying that there exists no steady-state solution for an isolated magnetic island in a co-moving frame. Of course, the solution to the "paradox" is quite simple. When we solve the *transport equation* which determines the velocity profile around the island [e.g., Eq. (42)], we find that only *one* of the solutions—corresponding to a particular island phase velocity—is localized (see Sec. II E). The remaining solutions are nonlocalized, and must, therefore, be rejected for an isolated island. Hence, the constraint (50), which is equivalent to the requirement that the island velocity profile be localized, really does uniquely determine the island phase velocity.

Finally, Ottaviani *et al.* have recently published a paper which demonstrates the existence of *two* different types of drift-MHD magnetic islands.[10] The first type is wide, and propagates slowly (in the local $\mathbf{E}\times\mathbf{B}$ frame). (Note that Ottaviani *et al.* only consider cold ions.) The second type is narrow, and propagates close to the electron diamagnetic velocity (in the local $\mathbf{E}\times\mathbf{B}$ frame). From the description of the two island types given by Ottaviani *et al.*, it is clear that the islands discussed in our paper are of the first type, and that islands of the second type are restricted to the thin island regime, $W \sim d_\beta$, which is not considered in this paper.

IV. NUMERICAL RESULTS

A. Description of code

Equations (6)–(9) have been solved numerically in an initial-value, finite-difference code, which is second order in both space and time. The code employs a fully implicit, multigrid, time-stepping algorithm constructed using the Portable, Extensible Toolkit for Scientific Computing (PETSc).[11]

The domain of solution is $x=[-1,+1]$ and $y=[-l/2, +l/2]$. The initial equilibrium is a Harris pinch with a uniform pressure gradient: $\psi=-b\ln[\cosh(x/b)]$, $Z=-[V_*/(1+\tau)]x$, $\phi=0$, and $V_z=0$. (Note that Z plays the role of pressure in our equations.) The system is periodic in the y direction. The boundary conditions in the x direction are that the values of ψ, Z, V_z, $\nabla^2\psi$, $\nabla^2\phi$, $\nabla^2 Z$, and $[\phi,Z]$ are held constant at $x=\pm 1$. The value of ϕ at $x=\pm 1$ is continuously

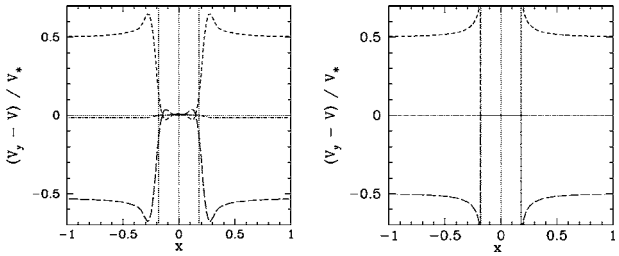

FIG. 2. Steady-state velocity profiles across the O-point of a subsonic island, in the island rest frame, normalized to the total diamagnetic velocity. The short-dashed, dot-dashed, and long-dashed curves show the ion fluid, $\mathbf{E}\times\mathbf{B}$, and electron fluid velocity profiles, respectively. The left-hand panel shows numerical results, whereas the right-hand panel shows the analytic prediction derived from Eqs. (41) and (46). The vertical dotted lines indicate the locations of the O-point (middle line) and the magnetic separatrix. Both calculations are performed with $l=8$, $b=0.6$, $\eta=10^{-3}$, $\mu_e=\mu_i=D=1.25\times10^{-4}$, $d_\beta=V_*=10^{-2}$, $c_\beta=1$, and $\tau=1$.

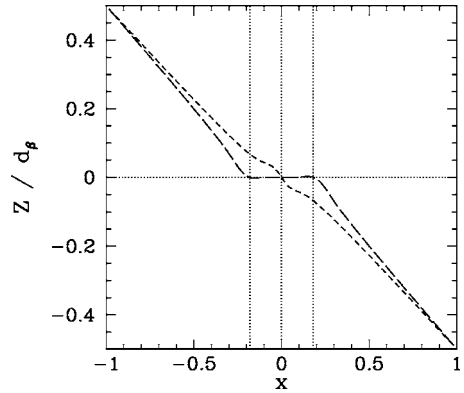

FIG. 3. Steady-state pressure profiles across the X- (short-dashed curve) and O- (long-dashed curve) points of a subsonic island. The vertical dotted lines indicate the locations of the O-point (middle line) and the magnetic separatrix (for the O-point profile). The calculation is performed with the same parameters as those used in Fig. 2.

adjusted so as to shift the calculation into a frame of reference which is co-moving with the island. This ensures that the calculation always asymptotes to a steady state. All of the calculations described in this paper are performed on a 128×128 grid.

B. Description of calculations

We use an equilibium ($l=8$, $b=0.6$) in which a single tearing mode of wavelength l is moderately unstable ($\Delta'=1.23$). The system is initiated in an equilibrium state, a small perturbation of wavelength l and amplitude 10^{-3} is added to the ψ field, and the system is then evolved in time until a steady state is achieved. Typically, with $\eta=10^{-3}$, this takes about 10^4 Alfvén times. The typical time step (which is kept fixed during each calculation) is about 10 Alfvén times.

C. Subsonic islands

Figure 2 compares the numerical and analytical velocity profiles, through the island O-point, of the ion, electron and $\mathbf{E}\times\mathbf{B}$ fluids, as measured in a frame of reference co-moving with the island. As can be seen, there is remarkably good agreement between the two. The only differences are that the numerical profiles show a very small level of fluid flow inside the island separatrix, whereas the analytic profiles predict zero fluid flow inside the separatrix. Furthermore, the numerical profiles resolve the boundary layer on the separatrix (in which the velocity profiles change rapidly), whereas this layer remains unresolved in our analytic profiles.

Figure 3 shows the pressure profiles across the island O- and X-points for the numerical calculation featured in Fig. 2. (Note that Z plays the role of pressure in our reduced equations.) It can be seen that the pressure profile is very accurately flattened across the island, in agreement with our analytic prediction [i.e., $dZ/d\psi\equiv L=L(\psi)$—see Sec. II D].

Figure 4 shows the island phase velocity as a function of the ratio μ_i/μ_e. It can be seen that there is very good agreement between the numerical results and the analytic prediction (47). It is certainly the case that when the (perpendicular) ion viscosity *exceeds* the (perpendicular) electron viscosity then the island propagates in the *ion* diamagnetic direction, and vice versa. The numerical results seem to asymptote toward the analytic prediction as the maximum values of μ_i and μ_e decrease. However, the agreement is better for islands propagating in the ion diamagnetic (i.e., $V-V_{EB}>0$), rather than the electron diamagnetic, direction. This discrepancy is probably due to momentum carried off by drift waves, which are preferentially emitted when the island propagates in the electron diamagnetic direction.[12]

Figure 5 shows the island phase velocity as a function of the diffusion parameter D. Again, it can be seen that the numerical results asymptote toward the analytic prediction (47) as D decreases. All in all, Figs. 4 and 5 indicate good agreement between numerical results and the analytic prediction (47), provided that the transport coefficients μ_i, μ_e, and D are sufficiently small.

Figure 6 shows the island phase velocity as a function of d_β (with a fixed ratio of V_*/d_β—which is equivalent to keeping the equilibrium pressure gradient fixed). The analytic for-

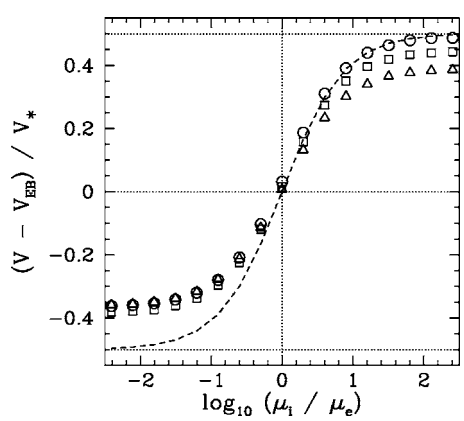

FIG. 4. Steady-state subsonic island phase velocity, V, in the local $\mathbf{E}\times\mathbf{B}$ frame, normalized to the total diamagnetic velocity, and evaluated as a function of μ_e/μ_i. The dashed curve shows the analytic prediction (47). The triangular points show numerical data with $\max(\mu_i,\mu_e)=2.5\times10^{-4}$ (i.e., μ_i is decreased while μ_e is held at 2.5×10^{-4} on the left-hand side of the graph, and vice versa on the right-hand side). The square points show numerical data with $\max(\mu_i,\mu_e)=1.25\times10^{-4}$. The circular points show numerical data with $\max(\mu_i,\mu_e)=6.25\times10^{-5}$. The calculations are performed with $l=8$, $b=0.6$, $\eta=10^{-3}$, $D=\max(\mu_i,\mu_e)$, $d_\beta=V_*=10^{-2}$, $c_\beta=1$, and $\tau=1$.

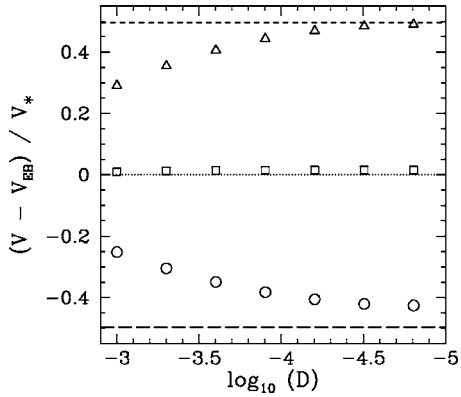

FIG. 5. Steady-state subsonic island phase velocity, V, in the local $\mathbf{E}\times\mathbf{B}$ frame, normalized to the total diamagnetic velocity, and evaluated as a function of D. The triangular points show numerical data with $\mu_e=4.883\times10^{-7}$ and $\mu_i=1.25\times10^{-4}$. The square points show numerical data with $\mu_e=1.25\times10^{-4}$ and $\mu_i=1.25\times10^{-4}$. The circular points show numerical data with $\mu_i=4.883\times10^{-7}$ and $\mu_e=1.25\times10^{-4}$. The short-dashed, dotted, and long-dashed lines show the analytic prediction (47) for these three cases, respectively. The calculations are performed with $l=8$, $b=0.6$, $\eta=10^{-3}$, $d_\beta=V_*=10^{-2}$, $c_\beta=1$, and $\tau=1$.

mula (47) predicts that $(V-V_{EB})/V_*$ should remain constant as d_β (and, hence, V_*) is increased. The numerical results shown in Fig. 6 verify this prediction.

Finally, Fig. 7 shows the saturated reconnected magnetic flux for the numerical calculations featured in Fig. 5. As d_β (and, hence, V_*) is increased, we expect the polarization term (2) in the Rutherford equation to also increase. (It should, in fact, increase quadratically with V_*). Moreover, according to (2), the polarization term is *stabilizing* for islands propagating in the *ion* diamagnetic direction, and *destabilizing* for islands propagating in the *electron* diamagnetic direction. The numerical results shown in Fig. 7 verify all of these predictions.

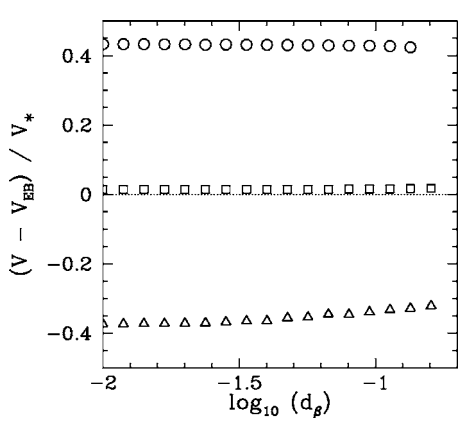

FIG. 6. Steady-state subsonic island phase velocity, V, in the local $\mathbf{E}\times\mathbf{B}$ frame, normalized to the total diamagnetic velocity, and evaluated as a function of d_β with a fixed ratio of V_*/d_β. The circular points show numerical data with $\mu_e=1.953\times10^{-6}$ and $\mu_i=1.25\times10^{-4}$. The square points show numerical data with $\mu_e=1.25\times10^{-4}$ and $\mu_i=1.25\times10^{-4}$. The triangular points show numerical data with $\mu_i=1.953\times10^{-7}$ and $\mu_e=1.25\times10^{-4}$. The calculations are performed with $l=8$, $b=0.6$, $\eta=10^{-3}$, $D=1.25\times10^{-4}$, $V_*=d_\beta$, $c_\beta=1$, and $\tau=1$.

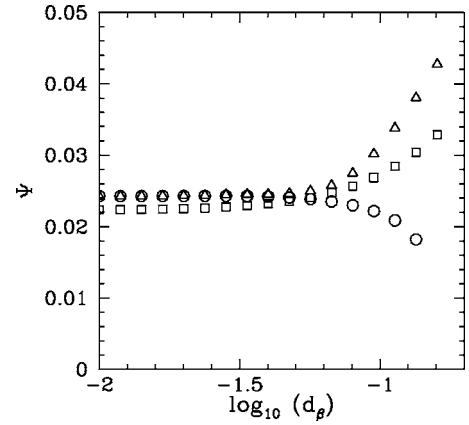

FIG. 7. Steady-state reconnected flux, Ψ, for a subsonic island, evaluated as a function of d_β with a fixed ratio of V_*/d_β. The data points and calculation parameters are the same as in Fig. 6.

D. Sonic islands

Figure 8 shows the island phase velocity as a function of the ratio μ_i/μ_e for various values of the sonic control parameter α [see Eq. (43)]. Note the very good qualitative agreement between the analytic predictions shown in Fig. 1, and the numerical results shown in Fig. 8. It certainly seems to be the case that as α is decreased, and we enter the sonic regime, the island phase velocity shifts towards the $\mathbf{E}\times\mathbf{B}$ velocity, with respect to the subsonic analytic prediction (47). Furthermore, the velocity shift is more marked for islands propagating in the ion diamagnetic (i.e., $V-V_{EB}>0$), rather than the electron diamagnetic, direction.

V. SUMMARY

Magnetic islands resulting from nonlinear tearing instabilities can seriously degrade the fusion plasma performance of magnetic confinement devices, such as tokamaks, which

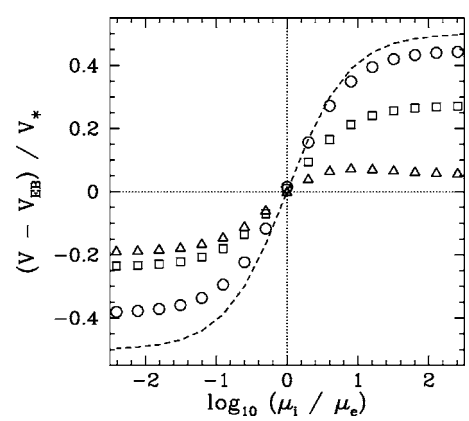

FIG. 8. Steady-state sonic island phase velocity, V, in the local $\mathbf{E}\times\mathbf{B}$ frame, normalized to the total diamagnetic velocity, and evaluated as a function of μ_e/μ_i. The dashed curve shows the subsonic analytic prediction (47). The circular points show numerical data with $c_\beta=1$. The square points show numerical data with $c_\beta=0.3161$. The triangular points show numerical data with $c_\beta=0.1$. The α values for these three cases are estimated to be 9, 2.8, and 0.9, respectively. The calculations are performed with $l=8$, $b=0.6$, $\eta=10^{-3}$, $\max(\mu_e,\mu_i)=1.25\times10^{-4}$, $D=1.25\times10^{-4}$, $d_\beta=V_*=2\times10^{-2}$, and $\tau=1$.

rely on the existence of nested toroidal magnetic flux surfaces. As is well known, the evolution of the island width is governed by a nonlinear equation due to Rutherford.[4] However, two-fluid and toroidal effects give rise to additional terms in this equation.[13] In particular, there is an important term, due to the ion polarization current, whose sign depends crucially on the island *phase velocity*. Hence, the determination of the phase velocity is a vital component of two-fluid magnetic island theory, since without this knowledge it is impossible to say whether the ion polarization term in the Rutherford equation is stabilizing or destabilizing.

Our investigation of the physics determining the phase velocity of magnetic islands is restricted to a *two-fluid* treatment in *slab geometry*, since it seems premature to us to attempt the far more difficult (but more realistic) kinetic approach in toroidal geometry without first gaining a thorough understanding of this comparatively elementary problem.

This paper only considers relatively *wide* islands for which $W \gg d_\beta$ (where d_β is equivalent to the well-known parameter ρ_s in a low-β plasma). There are two regimes of interest. In the *subsonic* limit, for which $kV_* \ll k_\parallel c_s$ [where V_* is the unperturbed local diamagnetic velocity, k the island wave number, $k_\parallel$ the parallel (to the magnetic field) wave number calculated at the edge of the island, and c_s the local sound speed], the propagation rate of sound waves around island flux surfaces is *much greater* than the island frequency (in the local $\mathbf{E}\times\mathbf{B}$ frame). In the *sonic* limit, for which $kV_* \sim k_\parallel c_s$, the propagation rate of sound waves around island flux surfaces is *similar* to the island frequency (in the local $\mathbf{E}\times\mathbf{B}$ frame).

In Sec. II, we present analysis which demonstrates that the phase velocity of a magnetic island in the subsonic and sonic limits is determined by *momentum transport* across the flux surfaces immediately outside the island separatrix. In the subsonic limit, the momentum transport is dominated by (perpendicular) *viscosity*. In the sonic limit, *Reynolds stresses*, which develop as a result of small pressure variations around flux surfaces driven by uneven cross-flux-surface transport, also play an important role. These pressure variations are smoothed out by sound waves in the subsonic limit.

In the subsonic limit, we obtain a very simple result. The island phase velocity is the (perpendicular) *viscosity weighted mean* of the unperturbed (i.e., in the absence of an island) local ion and electron fluid velocities. In the sonic limit, we find that the phase velocity shifts toward the local unperturbed $\mathbf{E}\times\mathbf{B}$ velocity with respect to the subsonic result.

We have performed a large number of non linear, 2D, drift-MHD simulations to investigate the propagation of saturated magnetic islands in two-fluid plasmas with diamagnetic flow. The results of these simulations, which are described in Sec. IV, are in remarkably good agreement with our analytic predictions.

The two-fluid slab model described in this paper should, hopefully, provide a firm foundation for future investigations of toroidal and kinetic influences on magnetic island propagation.

ACKNOWLEDGMENT

This research was funded by the U.S. Department of Energy under Contract No. DE-FG05-96ER-54346.

[1] M. N. Rosenbluth, Plasma Phys. Controlled Fusion **41**, A99 (1999).
[2] Z. Chang and J. D. Callen, Nucl. Fusion **30**, 219 (1990).
[3] A. I. Smolyakov, Plasma Phys. Controlled Fusion **35**, 657 (1993).
[4] P. H. Rutherford, Phys. Fluids **16**, 1903 (1973).
[5] H. P. Furth, J. Killeen, and M. N. Rosenbluth, Phys. Fluids **6**, 459 (1963).
[6] R. Fitzpatrick and F. L. Waelbroeck, Phys. Plasmas **12**, 022307 (2005).
[7] F. L. Waelbroeck, J. W. Connor, and H. R. Wilson, Phys. Rev. Lett. **87**, 215003 (2001).
[8] B. D. Scott, A. B. Hassam, and J. F. Drake, Phys. Fluids **28**, 275 (1985).
[9] A. B. Mikhailovskii, Contrib. Plasma Phys. **43**, 125 (2003).
[10] M. Ottaviani, F. Porcelli, and D. Grasso, Phys. Rev. Lett. **93**, 075001 (2004).
[11] S. Balay, V. Eijkhout, W. D. Gropp, L. C. McInnes, and B. F. Smith, "Efficient management of parallelism in object oriented numerical software libraries," in *Modern Software Tools in Scientific Computing*, edited by E. Arge, A. M. Bruaset, and H. P. Langtangen (Birkhäuser, Boston, MA, 1997), p. 163.
[12] F. L. Waelbroeck, J. W. Connor, and H. R. Wilson, Phys. Rev. Lett. **87**, 215003 (2001).
[13] O. Sauter, R. J. La Haye, Z. Chang *et al.*, Phys. Plasmas **4**, 1654 (1997).